

PHOTONICS

Bioinspired bright noniridescent photonic melanin supraballs

Ming Xiao,^{1*} Ziying Hu,^{2,3*} Zhao Wang,⁴ Yiwen Li,⁵ Alejandro Diaz Tormo,⁶ Nicolas Le Thomas,⁶ Boxiang Wang,⁷ Nathan C. Gianneschi,^{2,3,4†} Matthew D. Shawkey,^{8,9†} Ali Dhinojwala^{1†}

Structural colors enable the creation of a spectrum of nonfading colors without pigments, potentially replacing toxic metal oxides and conjugated organic pigments. However, significant challenges remain to achieve the contrast needed for a complete gamut of colors and a scalable process for industrial application. We demonstrate a feasible solution for producing structural colors inspired by bird feathers. We have designed core-shell nanoparticles using high-refractive index (RI) (~1.74) melanin cores and low-RI (~1.45) silica shells. The design of these nanoparticles was guided by finite-difference time-domain simulations. These nanoparticles were self-assembled using a one-pot reverse emulsion process, which resulted in bright and noniridescent supraballs. With the combination of only two ingredients, synthetic melanin and silica, we can generate a full spectrum of colors. These supraballs could be directly added to paints, plastics, and coatings and also used as ultraviolet-resistant inks or cosmetics.

INTRODUCTION

In the colorful world in which we live, colors are significant not only for aesthetics and pleasure but also for communication, signaling, and security. Colors are produced through either absorption of light by molecules (pigmentary colors) or scattering of light by nanostructures (structural colors) (1). Structural colors are superior to pigmentary colors in many ways, because of their tunability, resistance to (photo or chemical) bleaching, and reduced dependence on toxic materials. Many recent studies have demonstrated the use of self-assembly to produce photonic crystals that generate colors across the visible spectrum (2). However, we still face significant challenges. Many traditional structural colors are iridescent and thus are not useful for wide-angle displays. Recent examples of noniridescent structural colors lack sufficient color saturation in the absence of absorbing materials (carbon black, gold nanoparticles, or black polypyrrole) to reduce incoherent scattering (3–7). Core-shell nanoparticles with a shell refractive index (RI) similar to water have been used to tune the spacing between cores to achieve optimal scattering for noniridescent colors, but only in solution (8, 9). Although both bottom-up and top-down methods have been widely used (10–12), there is a demand for a scalable process for mass production of structural colors.

Nature provides many spectacular examples of structural colors, such as green-winged teal (*Anas crecca*) wing feathers that use hexagonal nonclose-packed melanosomes (13) and wild turkey (*Meleagris gallopavo*) feathers with hollow, high-RI contrast melanosomes that brighten feather colors (Fig. 1A) (14, 15). These examples inspire the design of

core-shell synthetic melanin nanoparticles (CS-SMNPs) described here, for the production of bright structural colors. Further driven by the demand for scalable production of structural colors, we have developed a facile one-pot reverse emulsion process to assemble CS-SMNPs into bright and noniridescent photonic supraballs. The use of melanin as the core material can increase the brightness and saturation of supraballs because of its unique combination of high RI and broadband absorption of light. In addition, melanin is biocompatible and can dissipate almost 90% of the ultraviolet (UV) radiation into heat within a nanosecond (16, 17), making those melanin-based supraballs suitable for cosmetics or UV-resistant inks.

RESULTS AND DISCUSSION

To design an optimal core-shell morphology for producing colors, we first used the FDTD (finite-difference time-domain) method to calculate the theoretical reflectance spectra (normal incidence) from the (111) plane of the most common photonic crystal with a face-centered cubic (FCC) packing composed of core-shell nanoparticles and homogeneous nanoparticles (see the Supplementary Materials for details). Relative to the lattice of homogeneous nanoparticles, the lattice of core-shell nanoparticles with high-RI cores and low-RI shells shows the maximum intensity at a similar wavelength but has higher reflectance (Fig. 1B). In contrast, the reverse core-shell structure consisting of low-RI cores and high-RI shells has a much lower reflectance than the lattice of homogeneous nanoparticles. These findings are consistent with previously reported photonic bandgap calculations (18). By varying the ratio of core-to-total radius, we find the highest reflectance (~130% relative to homogeneous nanoparticles) for high-RI core/low-RI shell structure when the core radius is ~60% of the radius of the whole core-shell nanoparticle. The lowest reflectance (~52% relative to homogeneous nanoparticles) for core-shell nanoparticles with low-RI cores is obtained when the core radius is ~80% of the whole core-shell nanoparticle (Fig. 1C). On the basis of these results, we designed nanoparticles with high-RI cores and low-RI shells to obtain higher reflectance and brighter colors.

We chose synthetic melanin as the core material because it has an unusual combination of high RI (~1.74) and broadband absorption in the visible spectral region that reduces incoherent scattering and thereby enhances color purity (19). We used silica (RI, ~1.45) as the

¹Department of Polymer Science, The University of Akron, Akron, OH 44325, USA.

²Department of Chemistry, Northwestern University, Evanston, IL 60208, USA.

³Materials Science and Engineering Program, University of California, San Diego, La Jolla, CA 92093, USA.

⁴Department of Chemistry and Biochemistry, University of California, San Diego, La Jolla, CA 92093, USA.

⁵College of Polymer Science and Engineering, State Key Laboratory of Polymer Materials Engineering, Sichuan University, Chengdu 610065, P. R. China.

⁶Photonics Research Group, Department of Information Technology, Ghent University–imec, Center for Nano- and Biophotonics (NB-Photonics), 9000 Ghent, Belgium.

⁷Institute of Engineering Thermophysics, Shanghai Jiao Tong University, Shanghai 200240, China.

⁸Evolution and Optics of Nanostructures Group, Department of Biology, The University of Ghent, 9000 Ghent, Belgium.

⁹Department of Biology and Integrated Bioscience Program, University of Akron, Akron, OH 44325, USA.

*These authors contributed equally to this work.

†Corresponding author. Email: ali4@uakron.edu (A.D.); matthew.shawkey@ugent.be (M.D.S.); nathan.gianneschi@northwestern.edu (N.C.G.)

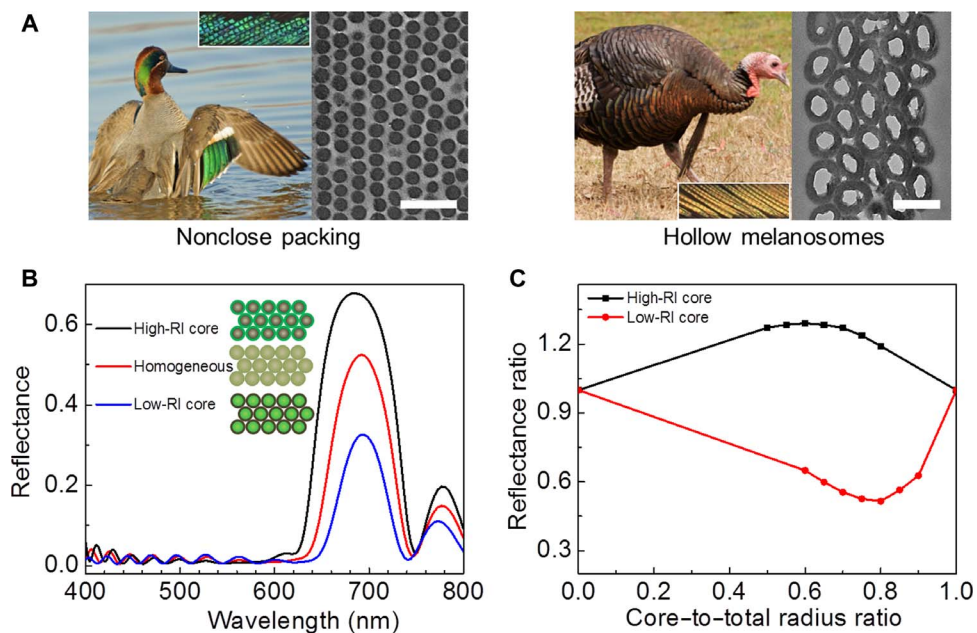


Fig. 1. Natural inspirations and the optical model. (A) Two biological examples to enhance color brightness: a green-winged teal (*Anas crecca*) wing feather and a cross-sectional transmission electron microscopy (TEM) image of a single barbule (left) and an iridescent wild turkey (*M. gallopavo*) wing feather and a cross-sectional TEM image of a single barbule (right). Scale bars, 500 nm. The photos of teal (credit to F. Pestana) and turkey (credit to T. Llovet) are from flickr.com under license numbers CC BY-SA 2.0 (<https://creativecommons.org/licenses/by-sa/2.0/>) and CC BY 2.0 (<https://creativecommons.org/licenses/by/2.0/>). (B) Normal reflectance spectra from the (111) plane of FCC lattices made of core-shell nanoparticles and homogeneous nanoparticles with similar sizes and equivalent refractive indices: high-RI core/low-RI shell nanoparticles (core: RI, 1.74; diameter, 200 nm; shell: RI, 1.45; thickness, 50 nm), equivalent homogeneous nanoparticles (RI, 1.54; diameter, 300 nm), and low-RI core/high-RI shell nanoparticles (core: RI, 1.45; diameter, 267 nm; shell: RI, 1.74; thickness, 16.5 nm). (C) The reflectance intensity ratio between core-shell and homogeneous structures changes as we vary the ratio of core radius to core-shell nanoparticle total radius.

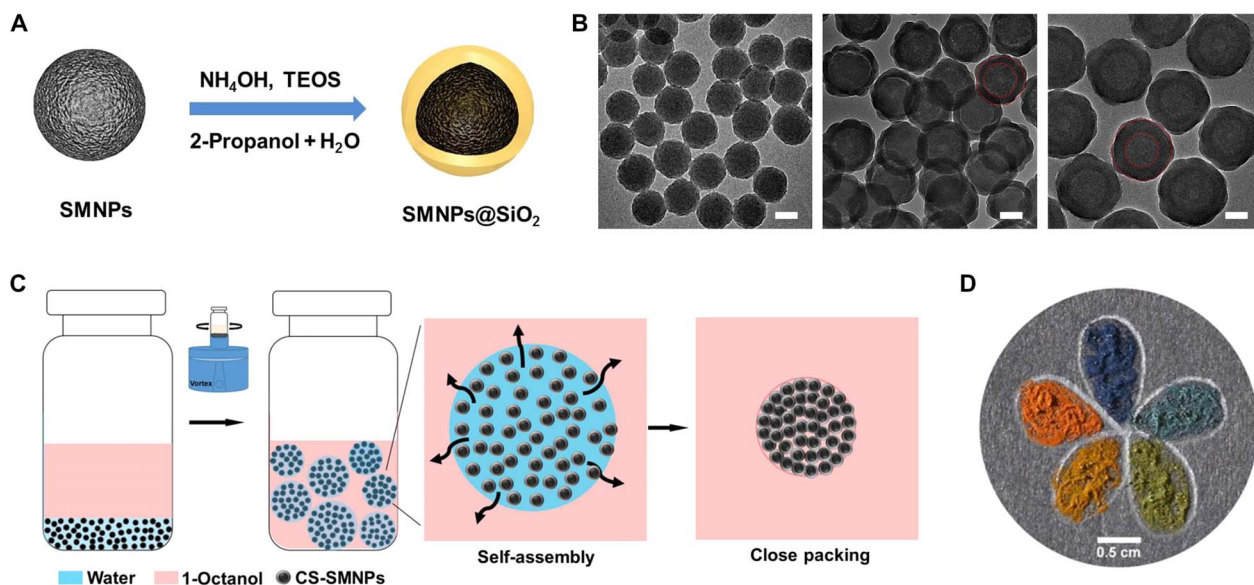


Fig. 2. CS-SMNP synthesis and self-assembly. (A) A scheme describing the method of synthesizing silica-coated melanin nanoparticles. (B) TEM images of CS-SMNPs: 160/0, 160/36, and 160/66 nm, respectively. The red dashed circles represent the boundary of the core and shell. Scale bars, 100 nm. (C) A scheme showing the self-assembly of supraball structures via a reverse emulsion process. (D) An image of rainbow-like flowers, painted with supraball inks made of five different sizes of CS-SMNPs: navy blue, 123/36 nm; blue-green, 123/43 nm; olive, 160/36 nm; orange, 160/50 nm; red, 160/66 nm.

low-RI shell and used a sol-gel reaction to coat it onto synthetic melanin cores, producing CS-SMNPs (Fig. 2A). We used synthetic melanin cores with diameters from 120 to 160 nm and tuned the coated shell thickness from 36 to 66 nm by adjusting the reaction time and sol-gel precursor concentration (table S1). In Fig. 2B, the core diameter of

160 ± 7 nm was kept constant, and the shell thickness was changed from 0 to 66 nm (for example, core diameter/shell thickness values of 160/0, 160/36, and 160/66 nm). By serving an analogous role to keratin in teal feathers, the shell helps to control the spacing between melanin nanoparticles.

We used a simple water-in-oil reverse emulsion template method to assemble CS-SMNPs into micrometer-sized supraballs ($51 \pm 14 \mu\text{m}$) (Fig. 2C) (20, 21). No surfactant molecules were used to stabilize the emulsion, and the transient stable emulsion droplets were formed upon shear mixing. The oil phase 1-octanol absorbed small amounts of water (20) and helped to reduce the amount of water in the aqueous phase containing CS-SMNPs. This process slowly removed the water and helped packing of CS-SMNPs into well-ordered supraballs. These supraballs produce a full spectrum of colors depending on the sizes of CS-SMNPs (Fig. 2D). This one-pot process is carried out at room temperature without additional posttreatment to remove water, and the supraballs can be easily separated by centrifugation. This process has a clear advantage over other emulsion-like processes used to produce colorful supraballs that require microwaves or heat to remove water (22–24). In contrast to microfluidic approaches, the reverse emulsion method is also easily scalable to produce larger quantities of supraball particles (5, 9, 25).

We investigated supraballs consisting of four types of nanoparticles. Under the stereomicroscope (mostly collecting scattering light), supraballs made of CS-SMNPs (160/36 and 160/66 nm) show highly visible olive and red colors, whereas supraballs made of 160/0-nm CS-SMNPs appear almost black (Fig. 3A). As a control, supraballs made of pure silica nanoparticles ($224 \pm 16 \text{ nm}$) display whitish cyan color. The reflectance spectra for individual supraballs contain one dominant peak in the visible spectral range located at ~ 430 , ~ 540 , and $\sim 660 \text{ nm}$ for supraballs composed of 160/0-, 160/36-, and 160/66-nm CS-SMNPs, respectively (Fig. 3B). The small variation in the curves from 12 different sizes of supraballs suggests that supraball size has no obvious

influence on color. The reflectance intensity of a single supraball increases with the thickness of the silica shell via reduced absorption by CS-SMNPs (fig. S1). The reflectance spectrum for silica particles has a dominant peak near 465 nm and is superimposed by a high-intensity, broad background signal that leads to a whitish color. This broad background is due to higher incoherent scattering (24). The increase in light absorption and reduction in incoherent scattering of CS-SMNPs produce more saturated colors that are visible to the naked eye. In addition, these colors are noniridescent, with clear advantages in applications such as wide-angle photonic inks (Fig. 3C and movie S1).

We used electron microscopy to investigate the mechanistic basis of these colors. Scanning electron microscopy (SEM) results show that supraballs are spherical and composed of close-packed nanoparticles (Fig. 4A). High-resolution SEM images and two-dimensional fast Fourier transform power spectra reveal that the nanoparticles are quasi-ordered on the supraball outer surfaces (Fig. 4B). The quasi-ordered packing helps to reduce the iridescence observed in well-ordered crystalline supraballs (26). The spherical geometry of supraballs also leads to noniridescent colors (5). Cross-sectional TEM images show that supraballs are solid and filled with close-packed nanoparticles (Fig. 4C and fig. S2). This solid morphology likely prevents the supraballs from collapsing.

We compared our empirical results with theoretical predictions of colors of melanin-based supraballs using FDTD simulations. We modeled a flat FCC photonic crystal consisting of six layers and calculated the normal reflectance from the (111) crystal plane without considering the curvature of the supraball surface. To consider the absorption of melanin, we used the RI and extinction coefficient of SMNPs

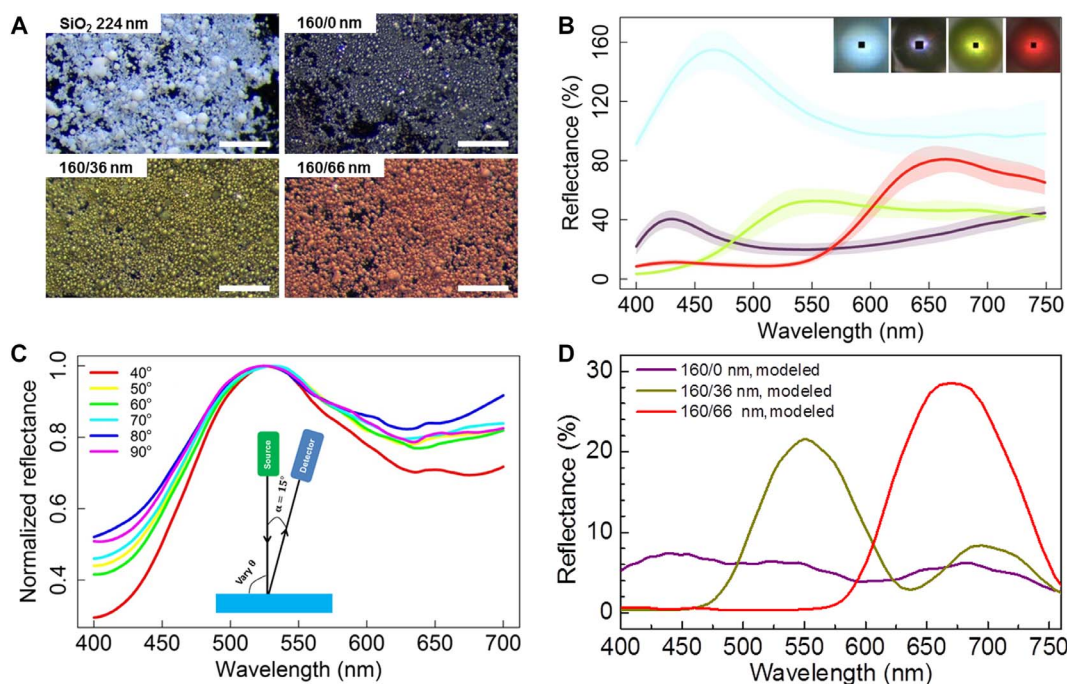


Fig. 3. Characterization of supraballs. (A) Optical images of supraballs made of four types of nanoparticles: 224-nm pure silica nanoparticles and 160/0-, 160/36-, and 160/66-nm CS-SMNPs. Scale bars, 0.5 mm. (B) Reflectance spectra and optical images for individual supraballs consisting of 224-nm pure silica nanoparticles (cyan curve, cyan supraball), 160/0-nm CS-SMNPs (purple curve, purple supraball), 160/36-nm CS-SMNPs (olive curve, olive supraball), and 160/66-nm CS-SMNPs (red curve, red supraball). The shaded area indicates the SD from 12 samples, plotted using pavo package in R (32). Each black box in the insets represents the size of the area probed by the optical measurements ($4 \times 4 \mu\text{m}$). (C) Angle-resolved spectra for olive inks, as shown in Fig. 2D. The inset scheme shows the setup for angle-resolved backscattering measurements where we fixed $\alpha = 15^\circ$ and varied angle θ between the source and the sample from 40° to 90° . (D) FDTD simulations of normal reflectance spectra from supraballs consisting of three different sizes of CS-SMNPs, where absorption of melanin was considered.

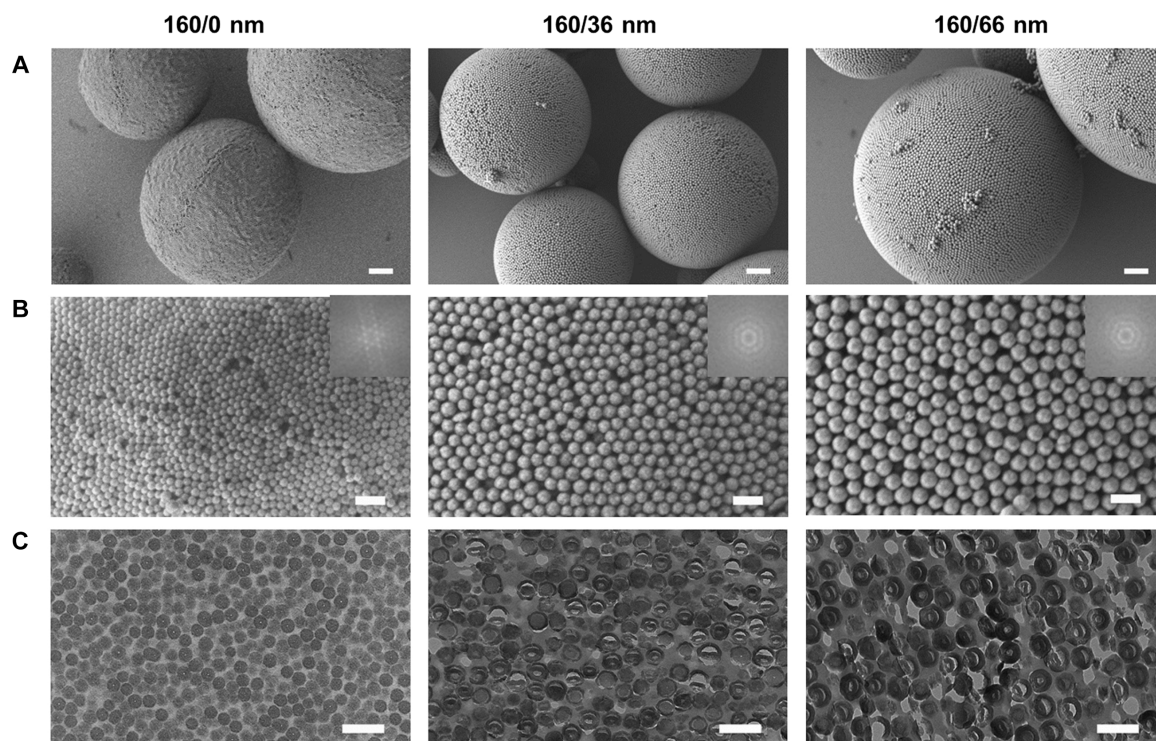


Fig. 4. Microstructures of supraballs. Each column represents supraballs made of different sizes of CS-SMNPs. (A) SEM images of whole supraball morphologies. (B) High-resolution SEM images of top surfaces of supraballs. (C) Cross-sectional TEM images of the inner structure of supraballs. Scale bars, 2 μm (A), 500 nm (B), and 500 nm (C).

reported in our previous publication (fig. S3A) (19). Incorporation of absorption terms in the simulation does not shift the peak position but only reduces the reflectance intensity to a different extent, depending on the volume ratio of melanin cores (fig. S3B). The calculated spectra for the supraballs contain a maximum peak position at ~ 440 , ~ 550 , and ~ 670 nm for 160/0-, 160/36-, and 160/66-nm CS-SMNPs, respectively (Fig. 3D). These predictions are in close agreement with the experimental measurements shown in Fig. 3B. The simulated spectra appear narrower than the experimental measurements because we use a flat perfect photonic crystal in our calculations, which is a simplified model for the structure we have in our experiments. However, the agreement with the maximum peak position indicates that this simple model is able to capture the origin of colors of these supraball structures.

Analogous to tuning pigmentary colors by mixing two types of pigments, we used the same reverse emulsion process to assemble CS-SMNPs with binary sizes (same core diameter but different shell thicknesses) into supraballs. Mixing pure SMNPs and CS-SMNPs with different shell thicknesses at a mass ratio of 1:1 resulted in a purple color similar to those produced by pure SMNP supraballs (Fig. 5, A and B, and fig. S4A, spectra). Both the SEM images of supraball outer surfaces and cross-sectional TEM images of supraballs demonstrate that only pure SMNPs segregate to the surfaces after mixing with CS-SMNPs (Fig. 5, A and B). However, mixing two sizes of CS-SMNPs with 1:1 ratio by mass results in an orange color (Fig. 5C and fig. S4B), and nanoparticles of both sizes of CS-SMNPs are randomly mixed at the surface and in the bulk (fig. S5). The differences in blending and segregation of nanoparticles can be explained by the higher affinity of melanin than silica to the oil-water interface. Therefore, the addition of different ratios of CS-SMNPs enables us to tune colors without synthesizing new CS-SMNPs of different shell thicknesses (Fig. 5D and fig. S6, spectra).

To understand the color blending effect, we used the inverse of normalized transport mean free path $A = (k_0 l)^{-1}$ to calculate the scattering intensity of supraballs made of 160/36- and 160/66-nm CS-SMNPs (details are provided in the Supplementary Materials) (27, 28). Compared with the model that assumes only independent scattering (simple summation of Mie scattering), the scattering model based on short-range order not only better captures the features of measured spectra but also predicts the color change with the variation in the mixing ratio of binary CS-SMNPs (fig. S7). Although the model considering the short-range order cannot precisely predict the reflectance peak positions, it suggests that the interference effect from the short-range order is critical for the color production in supraballs made of mixed CS-SMNPs.

CONCLUSION

Inspired synergistically by nonclose packing of melanosomes in teal feathers and hollow melanosomes in turkey feathers, as well as theoretical FDTD modeling, we have designed CS-SMNPs that can self-assemble into micrometer-sized colorful supraballs through a one-pot, scalable reverse emulsion process. This control of spacing leads to supraballs with tunable colors across the entire visible spectrum. The structure of high-RI cores and low-RI shells increases reflectance to produce brighter colors. The use of melanin is critical to the success of this strategy because it provides the required RI contrast between the cores and the shells and the broad absorption that helps to enhance the color saturation by absorbing incoherent scattering. In addition to all the optical merits of using CS-SMNPs, the reverse emulsion method to fabricate supraballs is simple, fast, and easily scalable. Similar to mixing pigmentary colors, one can match a desired color by simply mixing binary CS-SMNPs. Therefore, this novel

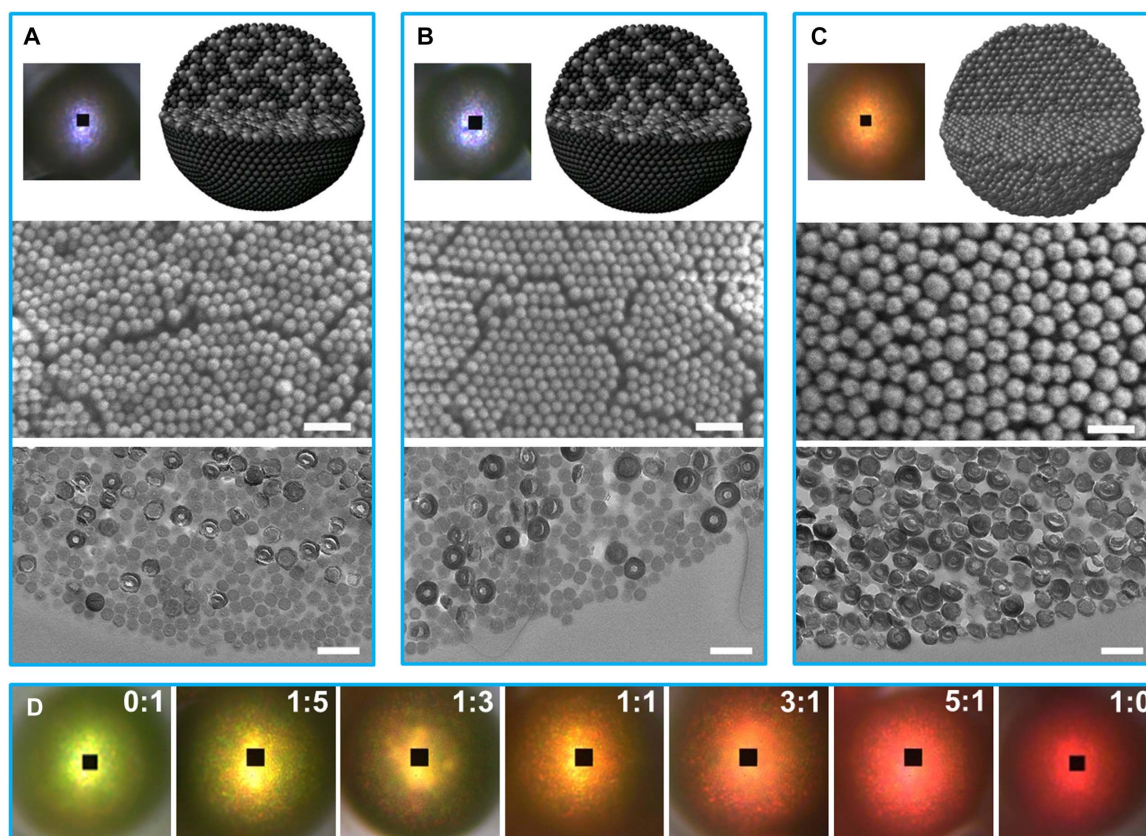


Fig. 5. Supraballs from binary CS-SMNPs. (A to C) Optical images, SEM images of top surface of supraballs, and cross-sectional TEM images for supraballs consisting of 160/0- and 160/36-nm CS-SMNPs (A), 160/0- and 160/66-nm CS-SMNPs (B), and 160/36- and 160/66-nm CS-SMNPs (C). The mixing ratio was 1:1 by mass. Top: Real images of supraballs made of mixed CS-SMNPs and sketches of supraballs, illustrating the organization of CS-SMNPs. Scale bars, 500 nm. (D) Optical images of supraballs prepared using different mass ratios of 160/36- and 160/66-nm CS-SMNPs. Each black box represents the size of the area probed by the optical measurements ($4 \times 4 \mu\text{m}$).

two-component strategy, melanin and silica, has the potential to revolutionize the use of structural colors in place of toxic organic- and metal-based pigments.

MATERIALS AND METHODS

Characterization of nanostructures in bird feathers

We obtained iridescent wild turkey (*M. gallopavo*) breast feathers and green-winged teal (*A. crecca*) wing feathers from the University of Akron collection. We followed our previous protocol to prepare barbule cross sections for TEM (29). Briefly, we dehydrated cut feathers using 100% ethanol and infiltrated them with 15, 50, 70, and 100% EMBED 812 resin (Electron Microscopy Sciences) every 24 hours. Next, we placed EMBED 812 resin and samples into block molds and cured them at 60°C overnight. We trimmed the blocks and cut 80-nm-thick sections on a microtome (Leica UC6, Leica Microsystems GmbH). Sections were placed onto copper grids for TEM imaging (JEM-1230, JEOL Ltd.).

Synthesis and characterizations of CS-SMNPs

We first synthesized pure SMNPs by oxidative polymerization of dopamine molecules (Sigma-Aldrich) under basic environment, following the procedure described in our previous work (19), and then deposited a silica shell (SiO_2) on the surface of SMNPs via the modified Stöber method (30). Typically, SMNPs (3.25 mg) were first dispersed in a mixture of 5-ml 2-propanol and 0.88-ml deionized water using an ultra-

sonic method followed by magnetic stirring. Then, 125 μl of ammonia solution (NH_4OH ; 28 to 30%) was added and stirred for 10 min. We controlled the amount of tetraethyl orthosilicate (TEOS) and hydrolysis reaction time to regulate the SiO_2 shell thickness (see details in table S1). Finally, CS-SMNPs were collected by centrifuge, washed three times with deionized water, and redispersed in deionized water for use in supraball preparation.

To examine the core-shell morphology and particle distributions, we drop-casted CS-SMNPs onto a carbon-coated copper grid for TEM (JEM-1230, JEOL Ltd.). We measured around 40 CS-SMNPs using ImageJ to obtain particle size and SD. We also measured the UV-visible (UV-vis) absorption of aqueous solutions of CS-SMNPs and solid silica particles using a UV-1800 UV-vis spectrometer (Shimadzu Corporation).

Supraball preparation

Typically, a solution of 30- μl aqueous CS-SMNPs with a concentration of 30 mg/ml was added to 1-ml anhydrous 1-octanol (Sigma-Aldrich). The water-in-oil emulsion formed rapidly using a digital vortex (Genie 2, Scientific Industries) at a shaking speed of 1600 rpm for 2 min. The shaking speed was then reduced to 1000 rpm for 3 min when supraballs were formed upon shrinking of the aqueous droplets, with water dissolving into the oil phase (20). After supraball sediments settled down, we removed most of the supernatant (0.9 ml) to concentrate the supraballs. Colorful supraballs were obtained by removing the 1-octanol at 60°C. In this method, it was also important to make the

glass vials hydrophobic so that aqueous droplets did not adhere to them and break upon contact. We coated an octadecyltrimethoxysilane (OTS) self-assembled monolayer (SAM) onto glass vials following a modified protocol (31). We added 2-volume % OTS toluene solution into dry and clean glass vials and degassed for 15 min before tightly closing the cap. After 16 hours at room temperature, we rinsed the vials three times with toluene and ethanol. Finally, the vials were annealed at 120°C under vacuum for 2 hours. To quantify whether OTS SAM was successfully grown onto glass vial, we put a clean glass slide inside the vial during the OTS growth and measured the contact angle of the glass slide (water contact angle, $112^\circ \pm 0.6^\circ$; fig. S8).

Supraball characterization

The dried supraballs were imaged under a Leica M80 stereo microscope (Leica Microsystems), and we used high-density Teflon tape (TaegaTech) as a white balance. The microscope contained light-emitting diode lights as the source and was connected to a Leica DMC 4500 camera. The reflectance spectrum of individual supraballs was measured using a CRAIC AX10 UV-vis-near-infrared microspectrophotometer (CRAIC Technologies Inc.), with a 75-W xenon short-arc lamp (Ushio UXL75XE) as a light source. We averaged spectra from 12 supraballs and calculated the SD using pavo package in R programming software (32). To investigate whether the colors of supraballs are angle-independent, we deposited thick films of supraballs and measured the scattering spectra from different angles using an AvaSpec spectrometer, with a xenon light source (Avantes Inc.) attached to a custom-built goniometer (Fig. 3C).

The nanostructure of supraball surfaces was characterized using a field-emission SEM (JEOL-7401, JEOL Ltd.). To investigate the inner structure of supraballs, we dispersed powders of supraballs into EMBED 812 resin in block molds and cured them at 60°C for 16 hours. The hard blocks were trimmed to a sharp trapezoidal tip using a Leica S6 EM-Trim 2 (Leica Microsystems), and we then cut 80-nm-thick sections using a diamond knife (Diatome Ltd.) on a Leica UC7 ultramicrotome for TEM.

SUPPLEMENTARY MATERIALS

Supplementary material for this article is available at <http://advances.sciencemag.org/cgi/content/full/3/9/e1701151/DC1>

Optical Model

table S1. Conditions used for synthesizing different sizes of CS-SMNPs.

fig. S1. UV-vis absorption spectra of pure SMNPs, CS-SMNPs, and pure silica nanoparticles in aqueous solution (20 mg/liter).

fig. S2. Representative TEM image of a small supraball made of 160/0-nm CS-SMNPs.

fig. S3. FDTD simulations of reflectance spectra at normal incidence using the dimensions of the core-shell particles in supraballs.

fig. S4. Comparisons of reflectance spectra collected for single supraballs made of melanin, core-shell nanoparticles, and mixtures of melanin and core-shell nanoparticles.

fig. S5. TEM images of the inner structure of supraballs of binary CS-SMNPs.

fig. S6. Normal reflectance spectra of supraballs made from 160/66- and 160/36-nm CS-SMNPs, and supraballs made by mixing different ratios of 160/66- and 160/36-nm CS-SMNPs.

fig. S7. Calculations of inverse of normalized transport mean free path as a function of different mixing ratios of 160/36- and 160/66-nm CS-SMNPs using the scattering theory outlined in SI.

fig. S8. Image of a drop of water on an OTS-coated glass.

movie S1. Supraball-painted flowers do not change colors when the sample is rotating at different angles.

References (33–44)

REFERENCES AND NOTES

- A. G. Dumanli, T. Savin, Recent advances in the biomimicry of structural colours. *Chem. Soc. Rev.* **45**, 6698–6724 (2016).
- J. F. Galisteo-López, M. Ibisate, R. Sapienza, L. S. Froufe-Pérez, Á. Blanco, C. López, Self-assembled photonic structures. *Adv. Mater.* **23**, 30–69 (2011).
- Y. Takeoka, S. Yoshioka, A. Takano, S. Arai, K. Nueangnoraj, H. Nishihara, M. Teshima, Y. Ohtsuka, T. Seki, Production of colored pigments with amorphous arrays of black and white colloidal particles. *Angew. Chem. Int. Ed.* **52**, 7261–7265 (2013).
- K. Katagiri, Y. Tanaka, K. Uemura, K. Inumaru, T. Seki, Y. Takeoka, Structural color coating films composed of an amorphous array of colloidal particles via electrophoretic deposition. *NPG Asia Mater.* **9**, e355 (2017).
- N. Vogel, S. Utech, G. T. England, T. Shirman, K. R. Phillips, N. Koay, I. B. Burgess, M. Kolle, D. A. Weitz, J. Aizenberg, Color from hierarchy: Diverse optical properties of micron-sized spherical colloidal assemblies. *Proc. Natl. Acad. Sci. U.S.A.* **112**, 10845–10850 (2015).
- X. Yang, D. Ge, G. Wu, Z. Liao, S. Yang, Production of structural colors with high contrast and wide viewing angles from assemblies of polypyrrole black coated polystyrene nanoparticles. *ACS Appl. Mater. Interfaces* **8**, 16289–16295 (2016).
- Y. Zhang, B. Dong, A. Chen, X. Liu, L. Shi, J. Zi, Using cuttlefish ink as an additive to produce non-iridescent structural colors of high color visibility. *Adv. Mater.* **27**, 4719–4724 (2015).
- S. Magkiriadou, J.-G. Park, Y.-S. Kim, V. N. Manoharan, Disordered packings of core-shell particles with angle-independent structural colors. *Opt. Mater. Express* **2**, 1343–1352 (2012).
- J.-G. Park, S.-H. Kim, S. Magkiriadou, T. M. Choi, Y.-S. Kim, V. N. Manoharan, Full-spectrum photonic pigments with non-iridescent structural colors through colloidal assembly. *Angew. Chem. Int. Ed.* **53**, 2899–2903 (2014).
- J. D. Forster, H. Noh, S. F. Liew, V. Saranathan, C. F. Schreck, L. Yang, J. G. Park, R. O. Prum, S. G. J. Mochrie, C. S. O'Hern, H. Cao, E. R. Dufresne, Biomimetic isotropic nanostructures for structural coloration. *Adv. Mater.* **22**, 2939–2944 (2010).
- J. Cui, W. Zhu, N. Gao, J. Li, H. Yang, Y. Jiang, P. Seidel, B. J. Ravoo, G. Li, Inverse opal spheres based on polyionic liquids as functional microspheres with tunable optical properties and molecular recognition capabilities. *Angew. Chem. Int. Ed.* **53**, 3844–3848 (2014).
- Z. Gan, M. D. Turner, M. Gu, Biomimetic gyroid nanostructures exceeding their natural origins. *Sci. Adv.* **2**, e1600084 (2016).
- C. M. Elison, M. D. Shawkey, A photonic heterostructure produces diverse iridescent colours in duck wing patches. *J. R. Soc. Interface* **9**, 2279–2289 (2012).
- C. M. Elison, P.-P. Bitton, M. D. Shawkey, How hollow melanosomes affect iridescent colour production in birds. *Proc. Biol. Sci.* **280**, 20131505 (2013).
- M. D. Shawkey, L. D'Alba, M. Xiao, M. Schutte, R. Buchholz, Ontogeny of an iridescent nanostructure composed of hollow melanosomes. *J. Morphol.* **276**, 378–384 (2015).
- J. B. Nofsinger, S. E. Forest, J. D. Simon, Explanation for the disparity among absorption and action spectra of eumelanin. *J. Phys. Chem. B* **103**, 11428–11432 (1999).
- A. Corani, A. Huijser, T. Gustavsson, D. Markovitsi, P.-Å. Malmqvist, A. Pezzella, M. D'Ischia, V. Sundström, Superior photoprotective motifs and mechanisms in eumelanins uncovered. *J. Am. Chem. Soc.* **136**, 11626–11635 (2014).
- K. P. Velikov, A. Moroz, A. van Blaaderen, Photonic crystals of core-shell colloidal particles. *Appl. Phys. Lett.* **80**, 49–51 (2002).
- M. Xiao, Y. Li, M. C. Allen, D. D. Deheyn, X. Yue, J. Zhao, N. C. Gianneschi, M. D. Shawkey, A. Dhinojwala, Bio-inspired structural colors produced via self-assembly of synthetic melanin nanoparticles. *ACS Nano* **9**, 5454–5460 (2015).
- O. Velev, K. Nagayama, Assembly of latex particles by using emulsion droplets. 3. Reverse (water in oil) system. *Langmuir* **13**, 1856–1859 (1997).
- D. Liu, F. Zhou, C. Li, T. Zhang, H. Zhang, W. Cai, Y. Li, Black gold: Plasmonic colloidosomes with broadband absorption self-assembled from monodispersed gold nanospheres by using a reverse emulsion system. *Angew. Chem. Int. Ed.* **54**, 9596–9600 (2015).
- S.-H. Kim, S. Y. Lee, G.-R. Yi, D. J. Pine, S.-M. Yang, Microwave-assisted self-organization of colloidal particles in confining aqueous droplets. *J. Am. Chem. Soc.* **128**, 10897–10904 (2006).
- H. Li, H. Wang, A. Chen, B. Meng, X. Li, Ordered macroporous titania photonic balls by micrometer-scale spherical assembly templating. *J. Mater. Chem.* **15**, 2551–2556 (2005).
- Y. Takeoka, S. Yoshioka, M. Teshima, A. Takano, M. Harun-Ur-Rashid, T. Seki, Structurally coloured secondary particles composed of black and white colloidal particles. *Sci. Rep.* **3**, 2371 (2013).
- S.-H. Kim, J.-G. Park, T. M. Choi, V. N. Manoharan, D. A. Weitz, Osmotic-pressure-controlled concentration of colloidal particles in thin-shelled capsules. *Nat. Commun.* **5**, 3068 (2014).
- O. D. Velev, A. M. Lenhoff, E. W. Kaler, A class of microstructured particles through colloidal crystallization. *Science* **287**, 2240–2243 (2000).
- M. C. W. van Rossum, T. M. Nieuwenhuizen, Multiple scattering of classical waves: Microscopy, mesoscopy, and diffusion. *Rev. Mod. Phys.* **71**, 313–371 (1999).
- P. Sheng, *Introduction to Wave Scattering, Localization and Mesoscopic Phenomena*, vol. 88 of *Springer Series in Materials Science* (Springer, 2006).
- M. Xiao, A. Dhinojwala, M. Shawkey, Nanostructural basis of rainbow-like iridescence in common bronzing *Phaps chalcoptera* feathers. *Opt. Express* **22**, 14625–14636 (2014).

30. W. Stöber, A. Fink, E. Bohn, Controlled growth of monodisperse silica spheres in the micron size range. *J. Colloid Interface Sci.* **26**, 62–69 (1968).
31. Y. Zhang, E. Anim-Danso, S. Bekele, A. Dhinojwala, Effect of surface energy on freezing temperature of water. *ACS Appl. Mater. Interfaces* **8**, 17583–17590 (2016).
32. R. Maia, C. M. Eliason, P.-P. Bitton, S. M. Doucet, M. D. Shawkey, pavo: an R package for the analysis, visualization and organization of spectral data. *Methods Ecol. Evol.* **4**, 906–913 (2013).
33. E. Akkermans, P. E. Wolf, R. Maynard, G. Maret, Theoretical study of the coherent backscattering of light by disordered media. *J. Geophys. Res.* **49**, 77–98 (1988).
34. D. S. Wiersma, P. Bartolini, A. Lagendijk, R. Righini, Localization of light in a disordered medium. *Nature* **390**, 671–673 (1997).
35. E. Akkermans, G. Montambaux, *Mesoscopic Physics of Electrons and Photons* (Cambridge Univ. Press, 2007).
36. M. Reufer, L. F. Rojas-Ochoa, S. Eiden, J. J. Sáenz, F. Scheffold, Transport of light in amorphous photonic materials. *Appl. Phys. Lett.* **91**, 171904 (2007).
37. L. Shi, Y. Zhang, B. Dong, T. Zhan, X. Liu, J. Zi, Amorphous photonic crystals with only short-range order. *Adv. Mater.* **25**, 5314–5320 (2013).
38. L. S. Froufe-Pérez, M. Engel, P. F. Damasceno, N. Muller, J. Haberko, S. C. Glotzer, F. Scheffold, Role of short-range order and hyperuniformity in the formation of band gaps in disordered photonic materials. *Phys. Rev. Lett.* **117**, 053902 (2016).
39. S. F. Liew, J. Forster, H. Noh, C. F. Schreck, V. Saranathan, X. Lu, L. Yang, R. O. Prum, C. S. O'Hern, E. R. Dufresne, H. Cao, Short-range order and near-field effects on optical scattering and structural coloration. *Opt. Express* **19**, 8208–8217 (2011).
40. L. Tsang, J. A. Kong, *Scattering of Electromagnetic Waves: Advanced Topics*, vol. 26 of *Wiley Series in Remote Sensing and Image Processing* (John Wiley & Sons, 2004).
41. M. S. Wertheim, Exact solution of the Percus-Yevick integral equation for hard spheres. *Phys. Rev. Lett.* **10**, 321–323 (1963).
42. C. F. Bohren, D. R. Huffman, *Absorption and Scattering of Light by Small Particles* (John Wiley & Sons, 2008).
43. C. Mätzler, MATLAB functions for Mie scattering and absorption: Version 2 (Research Report No. 2002-11, Institut für Angewandte Physik, 2002); www.atmo.arizona.edu/students/courselinks/spring09/atmo656b/maetzler_mie_v2.pdf.
44. A. Lagendijk, B. Nienhuis, B. A. van Tiggelen, P. de Vries, Microscopic approach to the lorentz cavity in dielectrics. *Phys. Rev. Lett.* **79**, 657 (1997).

Acknowledgments: We thank C. M. Eliason for providing the TEM images for duck and turkey feathers. We also thank A. S. Carlini for drawing the three-dimensional schemes of supraballs. **Funding:** This work was supported by the Air Force Office of Scientific Research (PECASE FA9550-11-1-0105 and FA9550-16-1-0331), NSF (EAR-1251895 and DMR-1105370), and Human Frontier Science Program (RGY-0083). **Author contributions:** M.X., Z.H., A.D., M.D.S., and N.C.G. designed the study. M.X., Z.H., Z.W., Y.L., and M.D.S. conducted the experiments. M.X., B.W., A.D.T., and N.L.T. ran the optical models. All authors contributed to the data interpretation and manuscript writing. **Competing interests:** M.X., Z.H., A.D., M.D.S., and N.C.G. are authors on a pending patent related to this work filed by the University of Akron (U.S. serial number 62/425285; filed on 22 November 2016). The other authors declare that they have no competing interests. **Data and materials availability:** All data needed to evaluate the conclusions in the paper are present in the paper and/or the Supplementary Materials. Additional data related to this paper may be requested from the authors.

Submitted 5 April 2017

Accepted 17 August 2017

Published 15 September 2017

10.1126/sciadv.1701151

Citation: M. Xiao, Z. Hu, Z. Wang, Y. Li, A. D. Tormo, N. Le Thomas, B. Wang, N. C. Gianneschi, M. D. Shawkey, A. Dhinojwala, Bioinspired bright noniridescent photonic melanin supraballs. *Sci. Adv.* **3**, e1701151 (2017).

Bioinspired bright noniridescent photonic melanin supraballs

Ming Xiao, Ziyang Hu, Zhao Wang, Yiwen Li, Alejandro Diaz Tormo, Nicolas Le Thomas, Boxiang Wang, Nathan C. Gianneschi, Matthew D. Shawkey and Ali Dhinojwala

Sci Adv 3 (9), e1701151.
DOI: 10.1126/sciadv.1701151

ARTICLE TOOLS

<http://advances.sciencemag.org/content/3/9/e1701151>

SUPPLEMENTARY MATERIALS

<http://advances.sciencemag.org/content/suppl/2017/09/11/3.9.e1701151.DC1>

REFERENCES

This article cites 39 articles, 5 of which you can access for free
<http://advances.sciencemag.org/content/3/9/e1701151#BIBL>

PERMISSIONS

<http://www.sciencemag.org/help/reprints-and-permissions>

Use of this article is subject to the [Terms of Service](#)

Science Advances (ISSN 2375-2548) is published by the American Association for the Advancement of Science, 1200 New York Avenue NW, Washington, DC 20005. 2017 © The Authors, some rights reserved; exclusive licensee American Association for the Advancement of Science. No claim to original U.S. Government Works. The title *Science Advances* is a registered trademark of AAAS.